Grey Area Mitigation for Detached-Eddy Simulations Using Volume Forcing

Antoine Monot, Christophe Friess, Jeroen Wackers

Grey area mitigation for Detached-Eddy Simulations using volume forcing

Antoine Monot[1], Christophe Friess[2], and Jeroen Wackers[1]

[1]Laboratoire de recherche en Hydrodynamique, Énergétique et Environnement Atmosphérique (LHEEA), CNRS UMR6598, École Centrale de Nantes

[2]Laboratoire de Mécanique, Modélisation & Procédés Propres (M2P2), CNRS UMR7340, Aix-Marseille Université, Centrale Marseille

Abstract

Hybrid RANS/LES (HRL) models are designed to allow transition between a RANS and a LES formulation inside the flow, ideally using LES only where it is necessary, and RANS otherwise, especially in complex regions like strong adverse pressure gradients. However HRL has issues when dealing with the transfer of the turbulent quantities usually coming from the RANS model to the LES part. The goal of this paper is to propose a solution to the lack of transition mechanism in the Detached-Eddy Simulation (DES) model and its subsequent iterations to handle the transfer of modeled to resolved turbulent kinetic energy (TKE) in the context of turbulent boundary layers. The presented approach uses a volume forcing based on Lundgren's method which amplifies already existing velocity fluctuations. The forcing is tuned so that the modeled TKE, which is dissipated by the DES method to transition to the LES mode, is compensated by generating the equivalent amount of resolved kinetic energy. The effectiveness of this solution is evaluated on a turbulent boundary layer over a flat plate, a geometrically simple case but the DES model is highly sensitive to mesh refinement in this configuration which allows for a precise evaluation of the forcing. Different meshes and time steps are tested to assess the impact of the method on the flow. This approach shows a clear improvement on the turbulent quantities inside the boundary layer when compared with the standard DES.

Keywords: Hybrid RANS-LES, Grey area, Volume forcing, DES

1 Introduction

A presentation of HRL models Since direct numerical simulations (DNS) and large eddy simulations (LES) are beyond reach for most industrial applications and RANS computations do not always offer a high enough level of precision especially when dealing with highly transient flow features, hybrid RANS-LES method arose as a viable intermediate between the low computational costs of RANS and the high fidelity of LES models. The core concept of these methods is to use a RANS

formulation whenever possible, mainly near solid boundaries where the very small size of eddies would force the use of a highly refined mesh to perform an accurate LES, while RANS models perform well. LES is used far away from the wall, mainly in regions with strong separations. Many different HRL models have been proposed such as the Detached-Eddy Simulation (DES) by Spalart et al. (1997), the Partially Averaged Navier-Stokes (PANS) model by Girimaji and Abdol-Hamid (2005) or the Partially Integrated Transport model (PITM) by Chaouat and Schiestel (2005).

The issue with the grey area Models like DES are known to have issues when dealing with attached or mildly separated flows, where most of the turbulence comes from the shear flow created by the boundary layer. The near-wall area, treated purely in RANS, only contains modeled turbulence which is supposed to be the source of the resolved turbulence further away from the wall, in the LES area. In the so-called grey area (GA) between RANS and LES, this modeled energy is destroyed to allow the creation of resolved eddies, so the modeled part of the energy spectrum gets smaller when the model reaches the well resolved LES. However, in flows without perturbation mechanisms in the outer flow, this creation does not occur, since DES has no built-in mechanism to convert the modeled energy into turbulent eddies. This causes a lack of turbulent energy, usually called modeled stress depletion (MSD).

DES is highly sensitive to the mesh resolution, since the transition from RANS to LES is based on the comparison of a turbulent length scale and the local mesh size. Therefore, DES meshes are usually constructed to minimize RANS-LES transitions in the boundary layer, which reduces MSD. However, HRL simulation is used for more and more complex flows and recent work like Mozaffari et al. (2022) shows that adaptive grid refinement (AGR) can improve the efficiency and accuracy of such computations. Still, AGR adapts the mesh to all flow features and cannot optimize only the boundary layer mesh. This means that for complex flows with multiple flow features, MSD in the boundary layer region appears inevitable.

Reducing MSD To solve this issue, multiple solutions have been proposed. The most common one for DES models is the use of a shielding function which prevents the RANS-LES transition inside the boundary layer. Thus the transition from pure RANS to well resolved LES is faster and more abrupt which facilitates the development of instabilities. Also the attached boundary layer is modeled entirely in RANS, which is suitable for these flows. The Delayed Detached-Eddy Simulations (DDES) (Spalart et al., 2006) and Improved Detached-Eddy Simulations (IDDES) (Shur et al., 2008) both add shielding functions to the DES model. This approach does not create a transfer from modeled to resolved turbulence, but it limits MSD by reducing the GA and improving its position in the flow.

Another way of handling MSD is to introduce an energy transfer viscosity term (Girimaji and Wallin, 2013) which decreases the turbulent viscosity of the flow so that instabilities develop faster. This method does not fit the role of a transfer mechanism either, but rather helps the development of natural instabilities. In configurations where few natural eddies exist (such as a turbulent boundary layer treated with a DES model) reducing the turbulent viscosity is often insufficient.

Turbulence forcing Active forcing methods are the most direct way to create the desired transfer of energy. These methods stimulate the appearance of resolved turbulence through fluctuating source terms in the momentum equations. While this is a natural idea, its implementation poses two challenges: selecting the right amount of forcing, and the correct spectrum of the fluctuations.

The issue of the forcing amplitude has been widely addressed in the literature. Many authors associate MSD with the commutation error between the filtering operator and partial derivatives (see e.g. Mehta et al. (2023); Arvidson et al. (2018); Rajamani and Kim (2010) among others). They estimate the commutation error, and use various techniques to generate the desired amount of fluctuations. While mathematically rigorous, these methods can be cumbersome to implement. Other approaches exist, such as Kok (2017) who uses a backscatter strategy to create the missing resolved TKE.

To create the fluctuations, different approaches have been proposed such as using precursor LES results from well-known flow configurations or downstream turbulence recycling (Lund et al., 1998). Both techniques use rescaled turbulence and prove to be efficient when the rescaling laws are correct. However these methods are constrained to simple flows and need significant user input to choose the right rescaling function. Synthetic turbulence generation (STG), which uses artificially computed turbulence, is another possible approach. One method of STG is the approach of Kraichnan (1970), which is based on a sum of random Fourier modes. The main issue with this method is its lack of simplicity, especially in assuring that the synthetic turbulence is compatible with the actual flow throughout a complex flow field.

The approach chosen in this paper is based on a forcing term that amplifies small pre-existing instabilities to generate eddies following the initial idea of Lundgren (2003). This use of turbulence extracted from the flow has the benefit of a low computational cost. The forcing is interpreted as a transfer of energy from modeled to resolved eddies, so its amplitude is derived from the artificial dissipation term which reduces the modeled turbulence during the transition from RANS to LES. To test the effectiveness of the approach for reducing MSD, it is intentionally developed for the original DES model, which is particularly sensitive to this issue. The proposed method is intended for use with adapted meshes (Mozaffari et al., 2022) on complex flows with vortex-boundary layer interaction (Visonneau et al., 2020). As such, its main objective is to reduce the mesh sensitivity of HRL turbulence models.

The paper is organized as follows. Section 2 describes the HRL model used, followed by the theory behind the artificial forcing method in section 3 which details the amplitude of the forcing and the targeted turbulent scales. The flat-plate boundary layer test case and numerical setup used are presented in section 4 and reference RANS / DES computations are shown in section 5. Detailed results of the DES model using the forcing method are presented in section 6, followed by a study of the model's sensitivity to variations of the mesh size and time discretization. The paper ends with a conclusion and a discussion of future improvements for the forcing.

2 The HRL model: DES

Both RANS and LES are based on the filtered incompressible Navier-Stokes equations:

$$\frac{\partial U_i}{\partial t} + \rho \frac{\partial U_i}{\partial x_j} = -\frac{\partial P}{\partial x_i} + \frac{\partial}{\partial x_j}\left(2\mu S_{ij} - \rho\overline{u_j' u_j'}\right), \tag{1}$$

$$\frac{\partial U_i}{\partial x_i} = 0. \tag{2}$$

These are obtained by introducing a decomposition $u = U + u'$ and $p = P + p'$, where U and P are the filtered velocity field and pressure field respectively. For RANS, this filter is the ensemble average, for LES it is a spatial average. The quantity $-\rho\overline{u_j' u_j'}$ is the subfilter-stress tensor which is given by the turbulence model, ρ the density of the flow, μ the molecular viscosity and S_{ij} the filtered strain-rate tensor.

DES-type HRL models create a bridge between RANS and LES by using the similarity of their respective formulations, thus any RANS model may be adapted to an HRL method. Since the k-ω SST model is a reliable RANS formulation for hydrodynamics and naval applications, which is the main targeted field of this work, only the SST version of the DES model (Strelets, 2001) will be used for this paper. While the ω transport equation is strictly identical to the original k-ω SST (Menter, 1993), the k transport equation has been modified to handle the additional dissipation of modeled energy required to switch from RANS to LES.

$$\frac{\partial \rho k}{\partial t} + \frac{\partial}{\partial x_j}\left(\rho U_j k - (\mu + \sigma_k \mu_t)\frac{\partial k}{\partial x_j}\right) = \tau_{ij}\frac{\partial U_i}{\partial x_j} - \underbrace{\beta^* \rho \omega k F_{DES}}_{\varepsilon^k_{DES}}. \tag{3}$$

The modified dissipation term of the DES model that dictates the mode in which the model is operating is detailed reads:

$$\varepsilon^k_{DES} = \rho\beta^* k\omega F_{DES}, \qquad \text{with:} \tag{4}$$

$$F_{DES} = \max\left(\frac{l_{k-\omega}}{C_{DES}\Delta_c}, 1\right), \text{the DES limiter,} \tag{5}$$

$$l_{k-\omega} = \frac{k^{1/2}}{\beta^*\omega}, \text{the RANS turbulence length scale,} \tag{6}$$

$$\Delta_c = \max\left(\Delta_x, \Delta_y, \Delta_z\right), \text{the mesh cutoff length scale.} \tag{7}$$

Following the idea of the original DES paper (Spalart et al., 1997), the modified dissipation term of the k transport equation is designed to ensure a RANS behavior if $F_{DES} = 1$ and a well resolved LES behavior when $F_{DES} > 1$ and the flow reaches equilibrium between the production and dissipation term. In this context, the model is equivalent to a Smagorinsky subgrid-scale model: $\nu_t \propto S\Delta^2$.

3 Forcing method theory

As will be shown in figure 3c, there is almost no resolved TKE in a turbulent boundary layer treated with DES. The total TKE shown in figure 3b contains only modeled energy. This example illustrates the lack of a mechanism designed to transfer the dissipated modeled energy into resolved energy.

The purpose of our forcing method is to create this mechanism in the DES model. The forcing converts modeled TKE into resolved TKE by generating instabilities inside the grey areas which occur near the transition from RANS to LES mode. This is achieved via a source term added to the Navier-Stokes equations (1).

3.1 Forcing amplitude

The main issue embedded in the design of DES, which was already anticipated in Spalart et al. (1997), is that while the behavior of the turbulence model is clear when $F_{DES} = 1$ (RANS) and when the flow is at equilibrium for $F_{DES} > 1$ (LES), the zone where $F_{DES} > 1$ and the flow is not at equilibrium (the grey area) does not bear a clear physical meaning. In this zone, the dissipation term in (3) assures both the physical dissipation of modeled turbulence and its artificial destruction to make way for resolved turbulence.

Our forcing is based on the assumption that this destruction in the grey area should not disappear, but must be reinjected as resolved turbulence to ensure the conservation of total TKE. Therefore, we break the dissipation term ε^k_{DES} down in two parts:

$$\varepsilon^k_{DES} = \varepsilon^k_{SGS} + \varepsilon^k_{tr}, \tag{8}$$

where ε^k_{SGS} is the physical dissipation of the sub-grid scale model and ε^k_{tr} the transfer dissipation of modeled to resolved energy.

Since a general expression for ε^k_{tr} is not available, equation 8 is detailed for three specific modes of the DES model:

1. In RANS mode ($F_{DES} = 1$), $\varepsilon^k_{SGS} = \beta^* \rho \omega k$ and $\varepsilon^k_{tr} = 0$. In this configuration ε^k_{DES} is known to be valid and concerns only the dissipation of modeled TKE since no resolved velocity fluctuations exist in the flow field.

2. In well established LES mode ($F_{DES} > 1$) the model is designed to function as a LES sub-grid scale turbulence model. Thus, k represents the sub-grid turbulence and the dissipation in the model represents its physical dissipation rate. Therefore, $\varepsilon^k_{SGS} = \beta^* \rho \omega k F_{DES}$ and once again, $\varepsilon^k_{tr} = 0$. In both these cases, no injection is required.

3. Lastly, at the very beginning of the grey area ($F_{DES} > 1$, but only modeled turbulence), k and ω still have the same values they had in the RANS zone. Thus, the physical dissipation is $\varepsilon^k_{SGS} = \varepsilon^k_{SST} \equiv \beta^* \rho k \omega$ and therefore $\varepsilon^k_{tr} = \varepsilon^k_{DES} - \varepsilon^k_{SST} = \beta^* \rho k \omega \, (F_{DES} - 1)$.

Within the grey area, the distribution of both transfer and SGS dissipation in equation (8) is not known. To handle this configuration, since most of the transfer is likely to occur close to the RANS zone, ε^k_{SST} can be used to approximate ε^k_{SGS} while the model is transitioning from RANS to LES at equilibrium. Thus:

$$\varepsilon^k_{tr} = \beta^* \rho k \omega \left(F_{DES} - 1 \right), \tag{9}$$

defines the target amount of energy injected in the flow.

However, given the actual dissipation term ε^k_{SGS} in the established LES zone, this first definition of ε^k_{tr} leads to an overestimation of the injection of turbulence. Therefore, a limiter is introduced as an attempt to avoid over-producing resolved TKE; this limiter estimates ε^k_{SGS} as the maximum between ε^k_{SST} and the production term $P^k = \tau_{ij} \frac{\partial U_i}{\partial x_j}$. For the computation of the injection, this leads to:

$$\varepsilon^k_{tr} = \rho \beta^* k \omega F_{DES} - \max \left(\rho \beta^* k \omega, P^k \right). \tag{10}$$

The choice of this limiter was made in order to recover the limit behavior of the DES model. Indeed, the model is designed to be equivalent to an algebraic sub-grid scale model like the Smagorinsky model when the flow reaches equilibrium meaning that the production and dissipation of turbulence are equal. In this flow state, ε^k_{DES} is equivalent to the modeled viscous dissipation of the flow and there should be no injection of TKE. The limiter allows the forcing method to respect this condition: when $P^k = \varepsilon^k_{DES}$ then $\varepsilon^k_{tr} = 0$, thus no body forces are applied if the flow reaches a balance between production and dissipation.

3.2 Targeted turbulent scales

When creating turbulence through momentum forcing, the turbulent scales affected by the forcing have a big impact on the efficiency of the creation of turbulent eddies. Thus, the chosen injection method should be able to target specific length and time scales. A common method of selecting the desired scales is to use synthetic velocity fluctuations, derived from an energy spectrum broken into multiple Fourier modes (Kraichnan, 1970). However this method requires a good knowledge of the flow field, since it requires accurate predictions of the energy cascade, taking into account that different flow behaviors result in different cascades.

Here the chosen approach is a modified Lundgren volume forcing (Lundgren, 2003), which is based on the amplification of pre-existing turbulence. The original goal of Lundgren's method is to sustain TKE in the flow in order to study stationary isotropic turbulence, thus it needs to be modified to fit the role of an energy transfer mechanism. This is done by redefining the amplifying coefficient so that it takes into account the additional dissipation of modeled kinetic energy ε^k_{tr}.

In Lundgren's method, a body force $f = AU'$ is added as a source term to the Navier-Stokes equations, where A is an amplifying coefficient based on the characteristics of the flow (see section 3.3) and U' a pre-existing velocity fluctuation of the flow field defined using a low-pass filter: $U = \overline{U} + U'$ with U the instantaneous velocity and $\overline{U}$ the filtered velocity. This method has shown to mainly impact scales

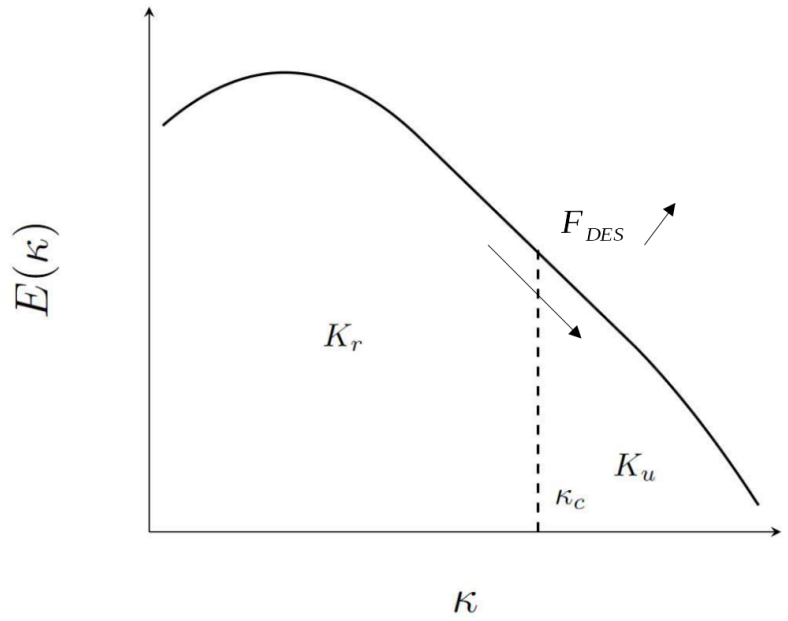

Figure 1: Turbulent cascade showing the distribution of resolved (K_r) and modeled (K_m) TKE based on the cutoff wavelength $\kappa_c = \pi/\Delta_c$. When F_{DES} increases, the resolved portion of the spectrum gets bigger.

between the integral scales and the inertial range (Rosales and Meneveau, 2005), so it focuses mainly on the large turbulent structures which are the scales where the lack of resolved turbulence takes place.

At time step n, U'^n is computed using an exponential averaging which acts as the low-pass filter:

$$\overline{U_i}^n = \alpha U_i^n + (1-\alpha)\,\overline{U_i}^{n-1}, \tag{11}$$

$$U_i'^n = U_i^n - \overline{U_i}^n. \tag{12}$$

This technique, also called exponentially-weighted average (Pruett et al., 2003), has many advantages compared to time or space averaging. A spatial average is only relevant for simple geometry flows where fluctuations can be considered statistically homogeneous in space, while a time average is only relevant for flows statistically stationary in time. The smoothing coefficient α gives an exponentially decreasing weight to the instantaneous velocity at a time step j as the current time step strays further from j. This gives more impact to the most recent characteristics of the flow while still not discarding the past flow behavior. This method acts as a low-pass filtering of the velocity signal with a fixed cutoff frequency (Cahuzac et al., 2010) dictated by the smoothing coefficient α and the time step:

$$f_c \propto \frac{\alpha}{\Delta t}(\mathrm{s}^{-1}). \tag{13}$$

Another advantage of the exponential average is that the parameter f_c can be used to select the scales which will be targeted by the Lundgren forcing. The importance of this is illustrated by figure 1 which shows the distribution of energy in the turbulence cascade between the resolved and filtered quantity. Suppose that a local variation of the mesh size occurs: the mesh is refined from Δ_1 to $\Delta_2 < \Delta_1$ as well as the associated cutoff wavelength κ_1 and $\kappa_2 > \kappa_2$. The theory presented

above says that the portion of the spectrum contained between these wavelengths should be converted from modeled to resolved energy. Ideally the low-pass filter $\langle U \rangle$ should remove these associated frequencies but keep the larger eddies. Thus, only the scales which are just large enough to be resolved on the mesh end up in U' and receive injected turbulence.

Therefore, variations of the time step and smoothing coefficient (α) have an impact on the forcing. To study this affirmation, in section 6.3 a first approach using a constant smoothing coefficient $\alpha = 0.01$ is chosen. Its value is then changed in multiple computations to observe its impact on the forcing. Ideally the value of α should dynamically change in space and time so that the cutoff frequency of the low pass filter and that of the flow are correlated.

3.3 Computation of the forcing

The turbulence injection approach is combined with a finite-volume discretization of the incompressible Navier-Stokes equations, with implicit time integration (see section 4.3 for details). The desired transfer TKE is injected in the momentum equation (1) via a volume force. Using the definition of the resolved TKE and the theory presented in section 3.1, the target added TKE in the time step $n+1$ is expressed as follows:

$$k_{target} = \varepsilon_{art}^{k} \Delta t = \frac{1}{2} \rho \left((\|U_i'^{n+1}\|)^2 - (\|U_i'^{n}\|)^2 \right), \tag{14}$$

with $\|U'^{n}\| = U_i'^{n} U_i'^{n}$ the amplitude of the velocity fluctuation at time step n and Δt the size of the time step. k_{target} is the amount of energy dissipated by ε_{art}^{k} over the course of the time step Δt.

From equation (14), the target velocity fluctuation at time step $n+1$ is obtained:

$$\|U_i'^{n+1}\| = \sqrt{\frac{2}{\rho} \varepsilon_{art}^{k} \Delta t + (\|U_i'^{n}\|)^2}. \tag{15}$$

The components of the velocity fluctuations and the components of the forcing are then computed as follows:

$$U_i'^{n+1} = U_i'^{n} \frac{\|U_i'^{n+1}\|}{\|U_i'^{n}\|}, \tag{16}$$

$$f_i = \rho \left(U_i'^{n+1} - U_i'^{n} \right) / \Delta t. \tag{17}$$

The velocity fluctuations are computed at the first non-linear iteration of each time step and the forcing term is not updated during the time step. Thus, the targeted velocity fluctuation is never truly reached. It is based on obsolete flow data when reaching the end of the time step's computation and the final velocity fluctuation is impacted by the rest of the Navier-Stokes equations. One way to circumvent this issue would be to introduce an implicit coupling between the forcing and the velocity computed with the momentum equation by recalculating the target velocity during the time step. However the current approach has the advantage of being more stable than this implicit formulation.

4 Test case: developing boundary layer over a flat plate

Attached boundary layers represent a difficult challenge for standard DES as the creation of turbulence is caused purely by wall friction in the RANS zone. Thus, they naturally cause significant modeled stress depletion (MSD) when the transition between RANS and LES occurs inside the boundary layer. This is therefore a logical test case to evaluate the quality of the forcing method: as the LES region contains no natural fluctuations, the forcing is responsible for the creation of all resolved turbulent content.

This section describes the computational domain and physical setup used in this paper. Reference results will be presented in section 5 and the forcing is tested in section 6.

4.1 Physical setup

The computational domain consists of a parallelepipedic volume of dimensions $L_x = 0.32$ m, $L_y = 0.1$ m and $L_z = 0.02$ m.

The fluid used is incompressible with density $\rho = 1000\ \mathrm{kg\,m^{-3}}$, dynamic viscosity 0.00104362 Pa s and an initial velocity of 70 $\mathrm{m\,s^{-1}}$ in the entire volume. A far field velocity of 70 $\mathrm{m\,s^{-1}}$ is applied at the inlet located at $x = 0$ m and at the top surface at $y = 0.1$ m. On the outlet located at $x = 0.32$ m a frozen pressure is applied. A no-slip condition is specified on the bottom wall at $y = 0$ m and mirror conditions are applied on both side surfaces at $z = -0.01$ m and $z = 0.01$ m. The undisturbed flow is turbulent: for both the top and the inlet surfaces, specified values of (modeled) turbulent kinetic energy (2.94 $\mathrm{m^2\,s^{-2}}$) and turbulent dissipation (18 $\mathrm{m^2\,s^{-3}}$) are imposed. The Reynolds number of this setup is around $2 \cdot 10^7$ based on the length of the flat plate.

4.2 Turbulence models and averaging strategy

As mentioned previously, the hybrid turbulence model used is the DES-SST developed by Strelets (2001). The k-ω SST RANS model accurately predicts the development of the boundary layers in this configuration. These results are used as a reference for all hybrid computations to estimate the right amount of turbulence that should be present.

To speed up the convergence and to reduce the impact of the convergence on the computation of the mean velocities, the DES-SST computations with forcing are started from a converged RANS solution on the same mesh and run until the average flow has converged. Finally, this computation is restarted to obtain the averaged flow used for post-processing.

4.3 Numerical setup

The flow solver used in this paper is the second-order unstructured finite-volume solver ISIS-CFD developed by Ecole Centrale de Nantes / CNRS (Queutey and Visonneau, 2007). This solver contains a SIMPLE-like pressure-velocity coupling. The discretization scheme used for turbulence and momentum is a blended scheme with 5% of 2nd order upwind and 95% of centered discretization. Diffusive fluxes use central discretizations and the implicit time integration is based on the two-step Adams-Bashforth scheme.

The mesh composed of stretched hexahedrons is purposely chosen to be ambiguous and to provoke a switch from RANS to LES inside the boundary layer, leading to significant MSD. Since the filter cutoff length is $\Delta_c = \Delta_{max} = \max(\Delta_x, \Delta_y, \Delta_z)$, its value is prescribed by the cell size along the streamwise direction (see table 1). Prismatic layers are used near the bottom wall surface to ensure $y^+ < 1$ in the first layer.

Name	$N_x \times N_y \times N_z$	Δ_x (m)	Δ_z (m)	N_{cells}	CFL
`x105`	$105 \times 81 \times 100$	$3.05 \cdot 10^{-3}$	$2 \cdot 10^{-4}$	850500	0.2295
`x210/z100`	$210 \times 81 \times 100$	$1.525 \cdot 10^{-3}$	$2 \cdot 10^{-4}$	1701000	0.459
`x420`	$420 \times 81 \times 100$	$7.625 \cdot 10^{-4}$	$2 \cdot 10^{-4}$	3402000	0.918
`x640`	$640 \times 81 \times 100$	$5 \cdot 10^{-4}$	$2 \cdot 10^{-4}$	5184000	1.4
`z25`	$210 \times 81 \times 25$	$1.525 \cdot 10^{-3}$	$8 \cdot 10^{-4}$	425250	0.459
`z50`	$210 \times 81 \times 50$	$1.525 \cdot 10^{-3}$	$4 \cdot 10^{-4}$	850500	0.459
`z200`	$210 \times 81 \times 200$	$1.525 \cdot 10^{-3}$	$1 \cdot 10^{-4}$	3402000	0.459

Table 1: Mesh variations of case `ts1e-5` (see table 2)

To study the effect of the spatial discretization on the forcing, multiple meshes with different refinement levels in the x and z directions are used. Table 1 shows all the mesh variations tested in this paper.

Name	Δt (s)	α	CFL	f_c (s^{-1})
`ts1e-5/a1e-2`	$1 \cdot 10^{-5}$	$1 \cdot 10^{-2}$	0.459	$1 \cdot 10^3$
`ts5e-6`	$5 \cdot 10^{-6}$	$1 \cdot 10^{-2}$	0.2295	$2 \cdot 10^3$
`ts2.5e-6`	$2.5 \cdot 10^{-6}$	$1 \cdot 10^{-2}$	0.1148	$4 \cdot 10^3$
`ts1e-6`	$1 \cdot 10^{-6}$	$1 \cdot 10^{-2}$	0.0459	$1 \cdot 10^4$
`ts5e-7`	$5 \cdot 10^{-7}$	$1 \cdot 10^{-2}$	0.02295	$2 \cdot 10^4$
`a5e-3`	$1 \cdot 10^{-5}$	$5 \cdot 10^{-3}$	0.459	$5 \cdot 10^2$
`a2.5e-3`	$1 \cdot 10^{-5}$	$2.5 \cdot 10^{-3}$	0.459	$2.5 \cdot 10^2$
`a1e-3`	$1 \cdot 10^{-5}$	$1 \cdot 10^{-3}$	0.459	$1 \cdot 10^2$
`a1e-2_ts5e-6`	$5 \cdot 10^{-6}$	$5 \cdot 10^{-3}$	0.2295	$1 \cdot 10^3$
`a2.5e-3_ts2.5e-6`	$2.5 \cdot 10^{-6}$	$2.5 \cdot 10^{-3}$	0.1148	$1 \cdot 10^3$
`a1e-3_ts1e-6`	$1 \cdot 10^{-6}$	$1 \cdot 10^{-3}$	0.0459	$1 \cdot 10^3$

Table 2: Time steps and α variations using mesh `x210` (see table 1)

The standard time step is equal to $1 \cdot 10^{-5}$ s and has been chosen to ensure that the CFL number stays below 1. Like the mesh, the impact of a varying temporal treatment of the turbulence is observed by changing the time step and the value of the smoothing coefficient α (equation (12), details in section 3.2). Table 2 presents the different configurations studied.

5 Reference computations

As a comparison for the forcing simulations in the following section, this section presents results for both RANS and standard DES-SST.

5.1 k-ω SST RANS

As mentioned earlier, the k-ω SST RANS model is reliable for attached boundary layers. Its mean quantities, mainly the turbulent kinetic energy and x velocity, are therefore used as references to estimate the quality of the presented forcing method. The reference results (figure 2) are computed on mesh `x210` and plotted in the z-centerplane, as well as a line located at $x = 0.3$m represented by the red line in figure 2a. Since the goal of the forcing is to compensate for a lack of turbulent kinetic energy in the flow, this quantity will be the main source of information to evaluate the forcing.

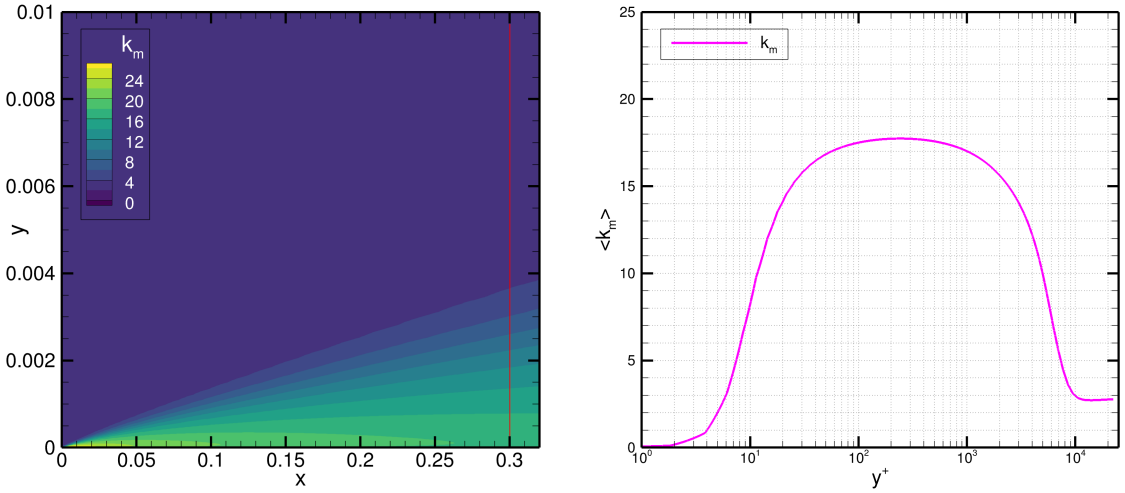

(a) Contour of TKE near the bottom wall

(b) TKE profile in the boundary layer ($x = 0.3$m)

(c) Contour of x velocity near the bottom wall

(d) x velocity profile of the boundary layer ($x = 0.3$m)

Figure 2: RANS results in the $z = 0$ centerplane, mesh `x210`

5.2 Standard DES-SST

As predicted in the introduction, without any form of external forcing the standard DES-SST model generates no resolved eddies. The increase of the k-dissipation term (equation (3)) reduces the modeled TKE, which decreases the turbulent viscosity. The underdevelopment of the boundary layer is a consequence of this.

Figure 3a shows the incomplete development of the boundary layer, compared with the RANS computation in figure 2a and 2c. Moreover, the freestream TKE far from the wall observed in the RANS computation disappears for the standard DES case (shown in figure 3b), leaving almost no TKE outside of the boundary layer.

Figure 3c shows the very small amount of resolved energy present in the flow. This implies that the TKE profile of figure 3b contains only the modeled energy. The TKE diminishes even in the zone where $F_{DES} = 1$ (figure 3d), so there is a two-way interaction between the RANS and LES zones.

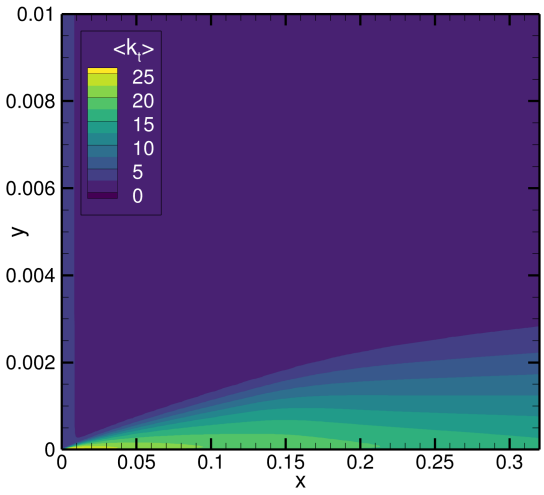

(a) Contour of the total TKE near the bottom wall

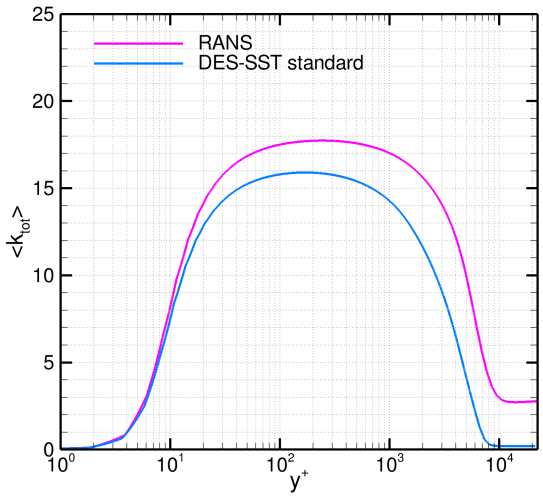

(b) Total TKE profile ($x = 0.3$m)

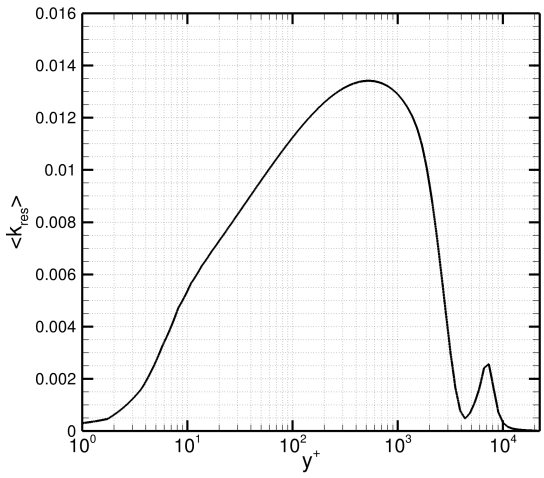

(c) Resolved TKE ($x = 0.3$m)

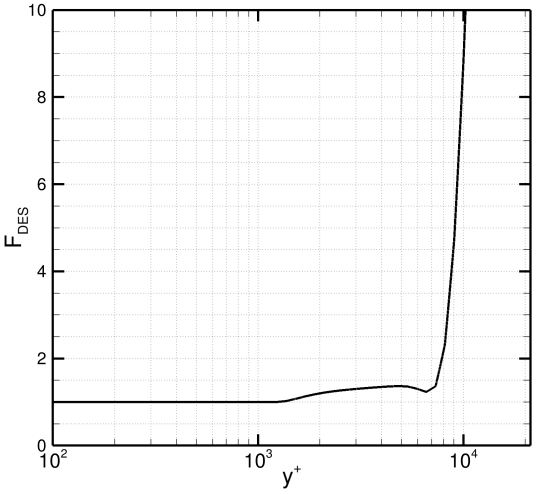

(d) F_{DES} profile ($x = 0.3$m). The y^+ axis is zoomed.

Figure 3: Standard DES results, mesh `x210`

Further tests, omitted here for brevity, show that different levels of mesh resolution or temporal discretization do not influence the amount of resolved turbulence in the

flow for a standard DES computation. Only the modeled energy varies according to the size of the RANS area: a coarser mesh will trigger the LES transition further away from the wall leaving more space to be modeled with the RANS model. Thus a coarse mesh will yield better results.

6 Forcing method results

The following section presents the results obtained when the forcing method described above is applied to the standard DES-SST model.

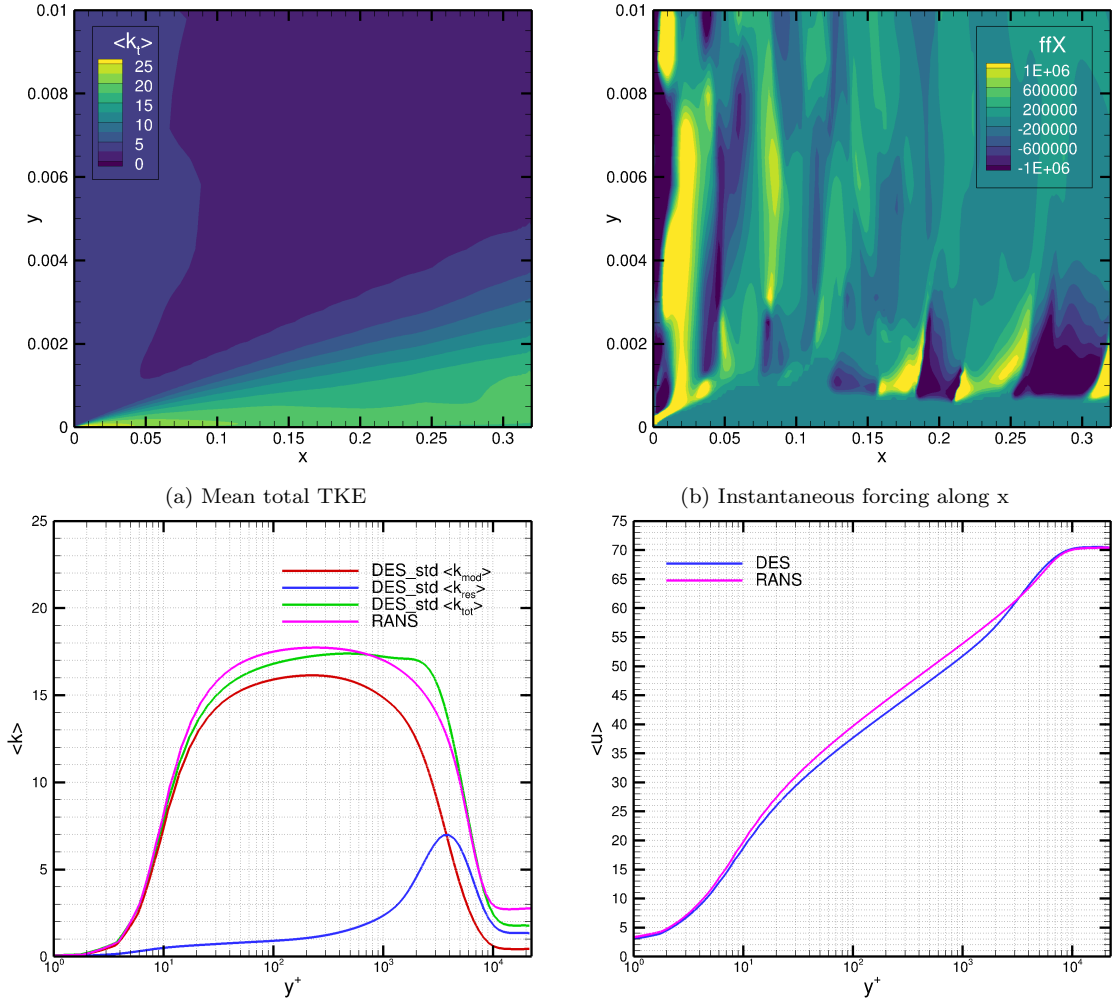

(a) Mean total TKE

(b) Instantaneous forcing along x

(c) Mean resolved, modeled and total TKE profiles

(d) Mean x velocity profile

Figure 4: DES with forcing, mesh `x210`

6.1 Initial forcing test

To illustrate the operation of the turbulence injection, a first simulation is analyzed. The mesh used for the results presented in this section is the `x210` case in table 1, the time integration setup is `ts1e-5+` / `a1e-2+` (table 2), and ε_{tr}^{k} is given by equation (9).

Figure 4b shows the instantaneous axial forcing f_x of equation (17). The body force has fairly large-scale fluctuations, and is strongest in the outer boundary layer region. As expected, in the near-wall RANS zone where $F_{DES} = 1$, the forcing is zero.

The forcing manages to generate enough fluctuations to match the TKE of the RANS computation (see figure 4c) with a slight overestimation of TKE right past the transition where the DES limiter starts increasing and, on the contrary, a slight underestimation of the near-wall turbulence. Although not all freestream turbulence is sustained, the forcing has converted the modelled inflow turbulence into resolved eddies, which is in line with the LES treatment of the outer flow. Overall, the simulation more accurately predicts the TKE in the flow.

Figure 4a shows the faster development of the boundary layer when compared to the standard DES (figure 3a), which matches well with the RANS computation. This is confirmed by the streamwise velocity profile in figure 4d which accurately follows the RANS profile.

The forcing method provides acceptable results with the current mesh and time step configuration. However the impact of varying spatial and temporal discretization, needs to be evaluated. Simulations with forcing contain much more resolved turbulence than RANS and 'natural' DES computations, but the mesh is too coarse to achieve a truly resolved LES, so the simulations are expected to be sensitive to the grid and the time step.

6.2 Spatial discretization

The impact of mesh refinement is studied by changing the cell size along the streamwise (x) or spanwise (z) direction. Since the entire boundary layer is meshed with multiple prismatic layers chosen to ensure that $y^+ < 1$ in the first layer, the mesh refinement along the y axis is unchanged. All the different meshes are presented in table 1 of section 4. The time integration setup used for all the mesh variations is the `ts1e-5` / `a1e-2` configuration presented in table 2, while ε_{tr}^k is given by equation (9).

Mesh variations along the streamwise direction First, the effects of different levels of mesh refinement along the streamwise direction on the computations and the forcing method are observed. This section uses meshes `x105`, `x210`, `x420` and `x640`. As mentioned earlier, the reference RANS computation uses mesh `x210`.

The most straightforward effect of the mesh variations is on the F_{DES} function profiles shown in figure 5a, which indicate the location of the RANS-LES transition. Since $\Delta_{max} = \max(\Delta_x; \Delta_y; \Delta_z)$ is always driven by Δ_x (see table 1), the finest meshes have transition regions closer to the wall compared to coarser meshes.

As shown in figure 5d and 5e, the varying location of the transition influences the balance between modeled and resolved energy. Coarser meshes tend towards a RANS behavior as a greater part of the boundary layer is treated by the RANS

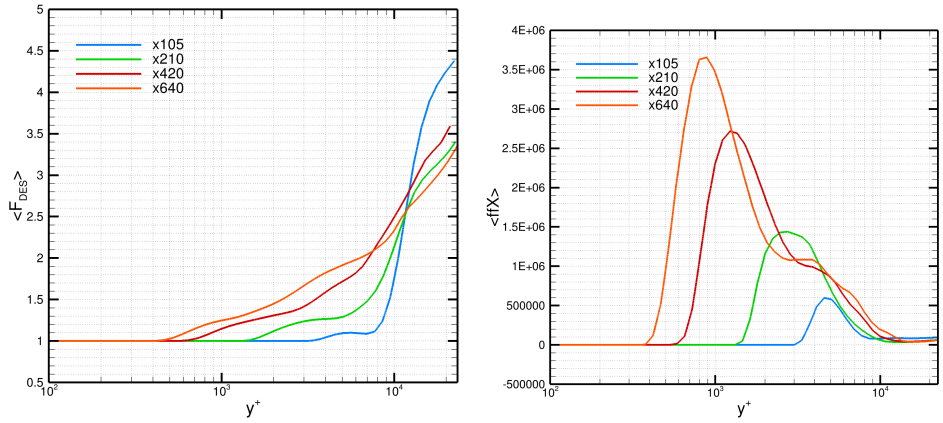

(a) Mean DES limiter

(b) Mean x forcing amplitude

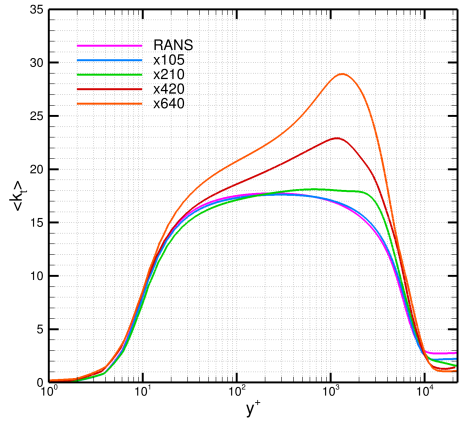

(c) Mean total TKE

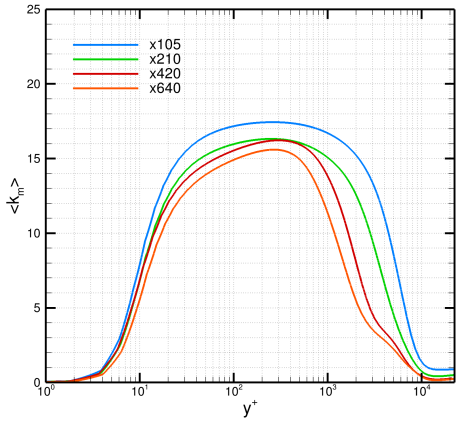

(d) Mean modeled TKE

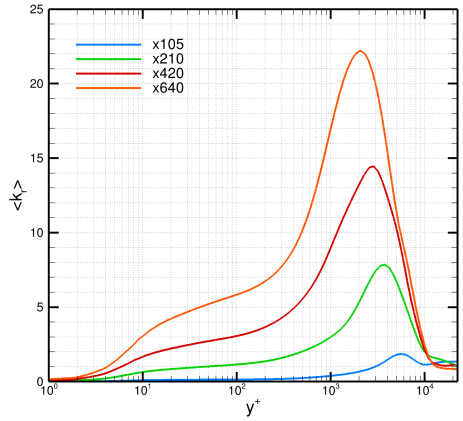

(e) Mean resolved TKE

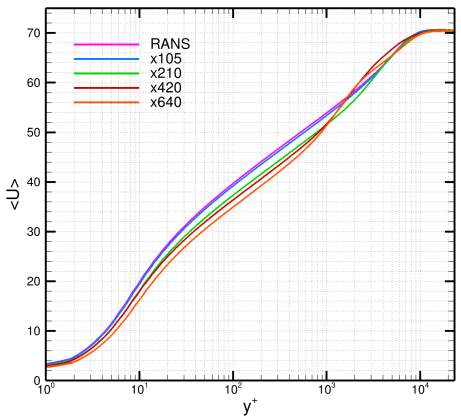

(f) Mean streamwise velocity

Figure 5: Streamwise resolution: profiles of mean F_{DES}, mean x forcing amplitude, streamwise velocity and resolved, modeled and total turbulent kinetic energy at $x = 0.3$m for meshes `x105`, `x210`, `x420` and `x640`

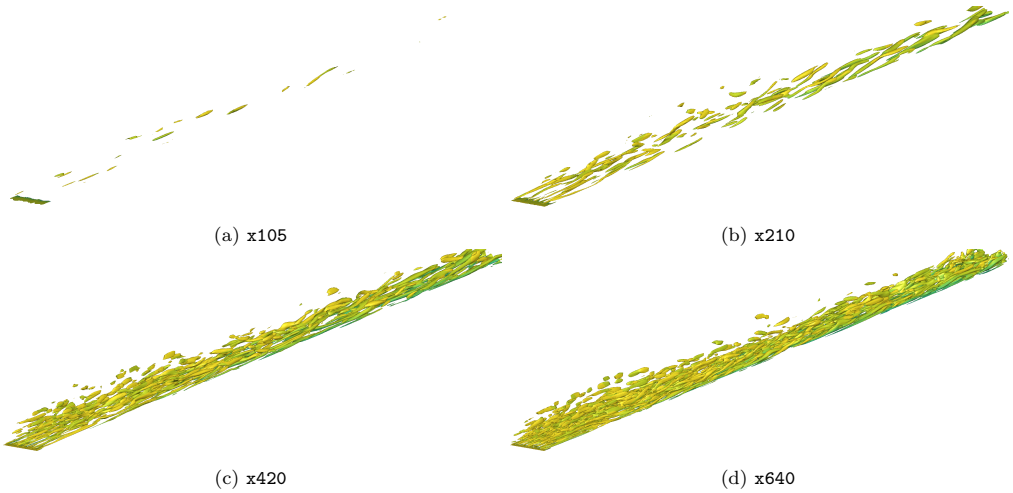

(a) x105 (b) x210

(c) x420 (d) x640

Figure 6: Streamwise resolution: $Q = 1 \cdot 10^6$ s^{-2} iso-surface for meshes x105, x210, x420 and x640

mode of the DES model. On the other hand, the LES behavior of finer meshes triggers closer to the wall. This generates more resolved TKE around the transition region and the amount of modeled TKE in the boundary layer gets lower.

The forcing method shows a progressively larger injection as the mesh is refined. Therefore, the total amount of turbulent kinetic energy shown in figure 5c becomes greater than the desired amount shown by the RANS computation. This is consistent with the theory in section 3: ε^k_{tr} according to equation (9) continues the ejection in the LES zone, so it should lead to an overestimation of the total TKE. The mean forcing amplitude (figure 5b) confirms this analysis. On finer meshes, the peak of the injection gets closer to the wall as expected, becoming progressively thinner and more intense. However, the injection stays strong throughout the boundary layer: there is more injection in the outer layer on the finest mesh than on the coarsest one.

Finally, the velocity profiles (figure 5f) on the finer meshes are less 'full' than the RANS profile. While the turbulence intensity on these meshes is too high, this turbulence does not create enough wall-normal momentum transport. The mesh, which is too coarse to represent near-wall turbulence in true LES fashion, may underestimate the velocity fluctuations in y-direction, independent of the forcing.

The Q-criterion $Q = 0.5\,(\Omega^2 - S^2)$, with Ω the vorticity tensor and S the strain rate tensor, shown in figure 6, indicates an increasing amount of vortices as the mesh is refined. While the scales for the injection (determined only by Δt and α) stay the same, the finer meshes show both stronger large-scale vortices and more fine eddies. This may have three causes: (i) the fine meshes cause more injection, (ii) the smaller cells are able to represent a wider part of the energy cascade, and (iii) the turbulent structures are better preserved over time thanks to a lower numerical diffusion. The tests below are intended to separate these elements.

Mesh variations along the spanwise direction Here the effects of different levels of mesh refinement along the spanwise direction on the computations and the forcing method are studied. The test uses meshes z25, z50, z100 and z200.

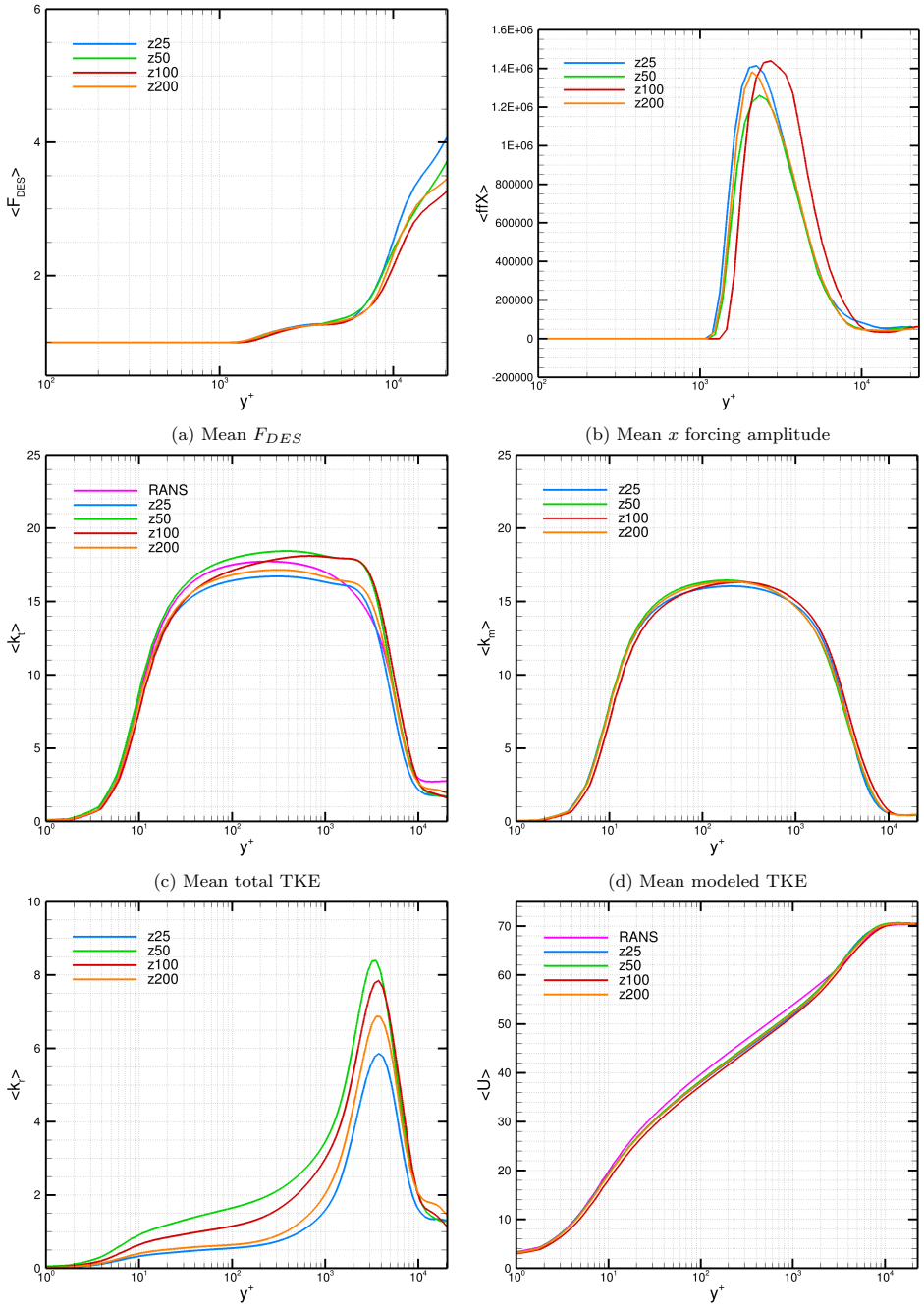

(a) Mean F_{DES}

(b) Mean x forcing amplitude

(c) Mean total TKE

(d) Mean modeled TKE

(e) Mean resolved TKE

(f) Mean streamwise velocity

Figure 7: Spanwise resolution: profiles of mean F_{DES}, mean x forcing amplitude, streamwise velocity and resolved, modeled and total turbulent kinetic energy at $x = 0.3$m for meshes `z25`, `z50`, `z100` and `z200`

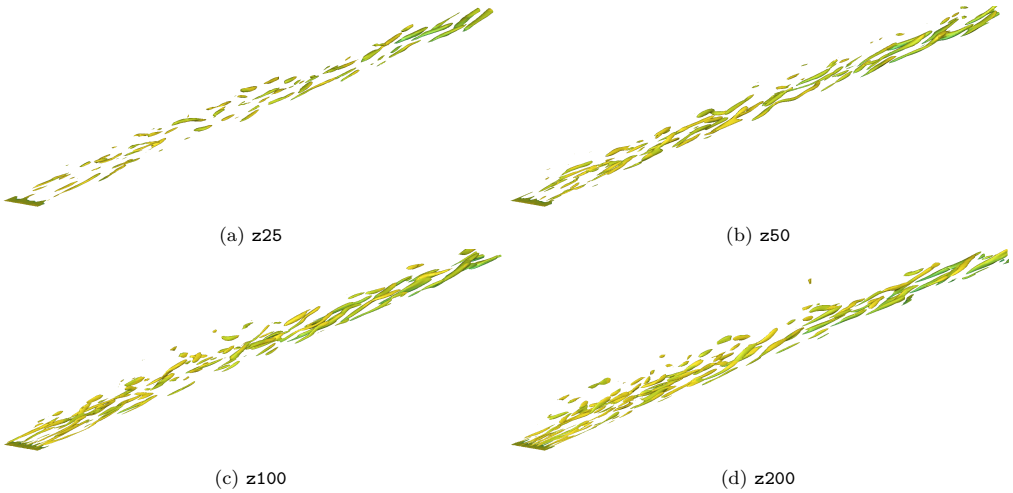

(a) z25 (b) z50

(c) z100 (d) z200

Figure 8: Spanwise resolution: $Q = 1 \cdot 10^6$ s^{-2} iso-surface for meshes z25, z50, z100 and z200

The goal of this test is to observe different levels of mesh refinement while keeping similar F_{DES} function profiles and identical positions of the RANS-LES transition point in the boundary layer. In this configuration Δ_{max} is constant. Even though Δ_z varies, it is always kept inferior to Δ_x, thus F_{DES} is nearly identical for all meshes (figure 7a). As a consequence, the RANS zone in the boundary layer has the same impact for all the computations, since the modeled turbulence hardly varies (figure 7d).

However the size of the RANS zone is not the only factor that influences the quality of the results. While the spanwise mesh variation study presents similar F_{DES} profiles, figure 7c still shows very different amounts of resolved TKE. In this case however, mesh refinement does not always imply an increase of TKE. Indeed figure 7e shows that while the mesh z50 displays more resolved turbulence than z25, the turbulence decreases from there on: even though z200 is better able to represent turbulence than coarser meshes like z50 and z100, less resolved energy is observed. Thus, a specific mesh size seems to maximize the amount of turbulence in the flow.

The Q-criterion in figure 6 and 8 again shows the presence of streamwise elongated turbulent streaks. While the Q-criterion on the coarsest mesh displays low amounts of turbulence, the finer meshes have a similar level of vortices, with some more small details on the finest mesh.

These observations confirm the discussion presented in section 3.2. There is a need for correlation between the exponential smoothing cutoff frequency and the mesh cutoff frequency. If the turbulent scales injected in the flow are too small for the resolution of the simulation (mesh z25) or too large to fit the highly stretched cells of mesh z200, the injection is inefficient. Furthermore, the mesh needs to suit the resolved turbulence; it is possible that the high aspect ratio cells degrade the resolved eddies.

6.3 Temporal discretization

The time step length and averaging parameter α have an effect on both the targeted frequencies for the injection, and on the accurate time evolution of turbulent structures (section 3.2). To study the impact of these parameters, the cases presented in table 2 have been simulated. They are divided in three main categories: variations of α, variations of the time step and variations of both parameters together so that the cutoff frequency (13) is preserved.

Figure 9 shows the turbulence kinetic energy. As the same mesh (`x210`) is used for all cases, little to no differences are found in profiles of k_m so only k_t and k_r profiles are shown. Figure 10 presents iso-surfaces of the Q-criterion for selected cases.

Reduction of the time step clearly reduces the resolved turbulence with a big gap between $2.5{\cdot}10^{-6}$ and $1{\cdot}10^{-6}$ seconds (figures 9a and 9b). Reducing Δt for constant α has the double effect of (i) increasing the temporal resolution, allowing smaller near-wall eddies to be captured, and of (ii) increasing the cutoff frequency of the exponential average. Thus, the TKE gets injected into these small eddies, which are barely resolved on the mesh and cannot stimulate the creation of larger eddies further from the wall. Figure 10b confirms that with a reduced time step, a kind of Tollmien-Schlichting instabilities appear instead of the streamwise elongated structures seen in previous computations (figure 10a).

On the other hand the decrease of parameter α, which decreases f_c without changing Δt, increases resolved turbulence (figures 9c and 9d). It should be noted that as α gets smaller, the time needed to stabilize the exponential average of the velocity increases, which is why the number of time steps was increased for all computations of this specific configuration. Still, the TKE profiles have similar behaviors and the shapes of the streaks are very close (figure 10c), which means that the resolved spectrum is more determined by the mesh and time step than by f_c. However, f_c has to agree with the mesh: if the turbulence is injected in scales that are too large for the mesh (c.f. figure 1), the total TKE gets overestimated, which is the case for $\alpha = 1 \cdot 10^{-3}$.

When both Δt and α vary (figures 9e and 9f), f_c stays constant and much smaller variations near the transition are observed. However, as the parameters decrease, the amount of resolved turbulence in the near-wall part of the boundary layer ($y^+ < 1000$) increases significantly. For $y^+ < 1000$, $F_{DES} = 1$ thus RANS mode is active in this area and there should be no velocity fluctuations. However, thanks to the turbulence cascade, some fluctuations stimulate smaller eddies in the RANS area, which can be resolved if the time step is small enough. These smaller eddies are visible in the Q iso-surface (figure 10d). The shapes of the total TKE profiles agree better with RANS when the parameters are reduced, which indicates that the propagation of resolved turbulence into the RANS area is actually needed to get correct results. As such, the overestimation in figure 9c may be caused by the resolved turbulence remaining 'blocked' in the larger eddies.

This behavior confirms that the cutoff frequency of the exponential smoothing has an important impact on the forcing both quantitatively and qualitatively, and

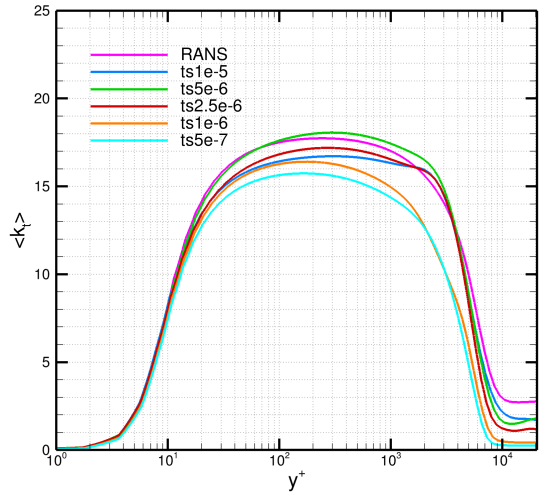

(a) $\langle k_t \rangle$, $\alpha = 1 \cdot 10^{-2}$

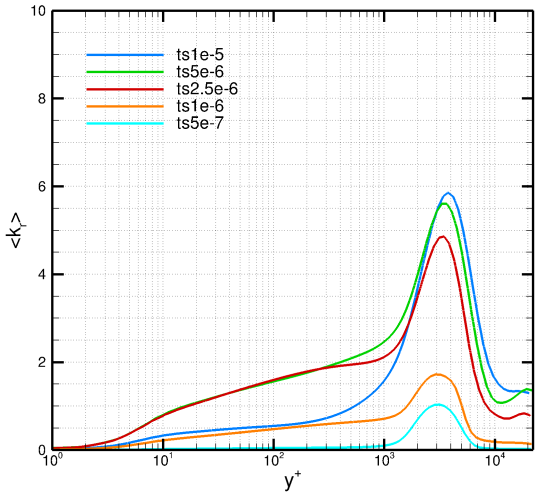

(b) $\langle k_r \rangle$, $\alpha = 1 \cdot 10^{-2}$

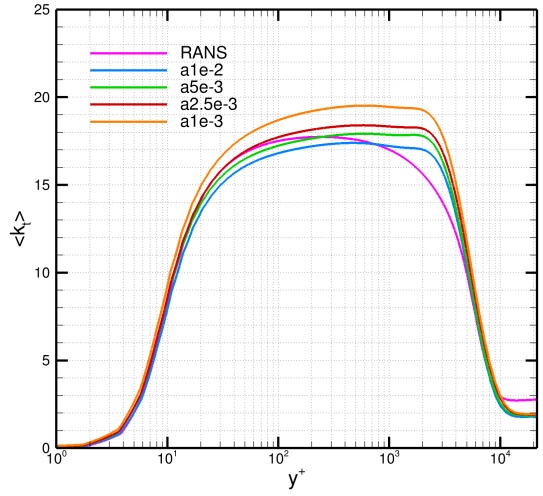

(c) $\langle k_t \rangle$, Time step $= 1 \cdot 10^{-5}$

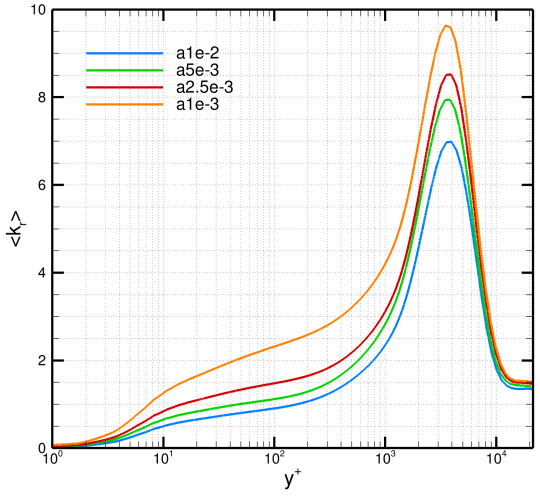

(d) $\langle k_r \rangle$, Time step $= 1 \cdot 10^{-5}$

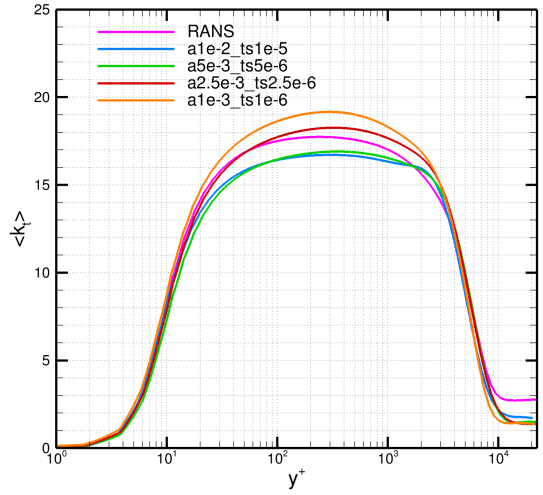

(e) $\langle k_t \rangle$, both α and the time step vary

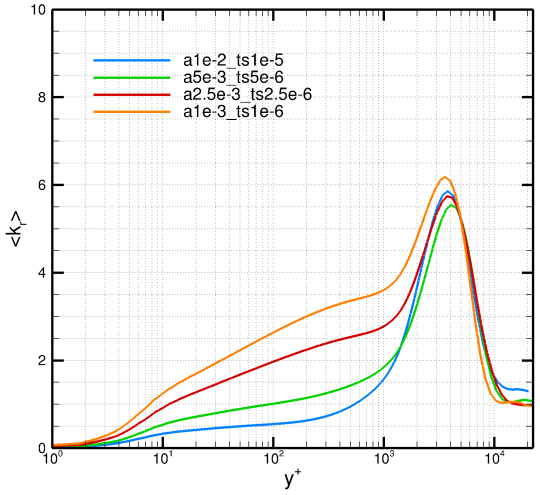

(f) $\langle k_r \rangle$, both α and the time step vary

Figure 9: Temporal discretization: total and resolved TKE profiles for variations of Δt and α

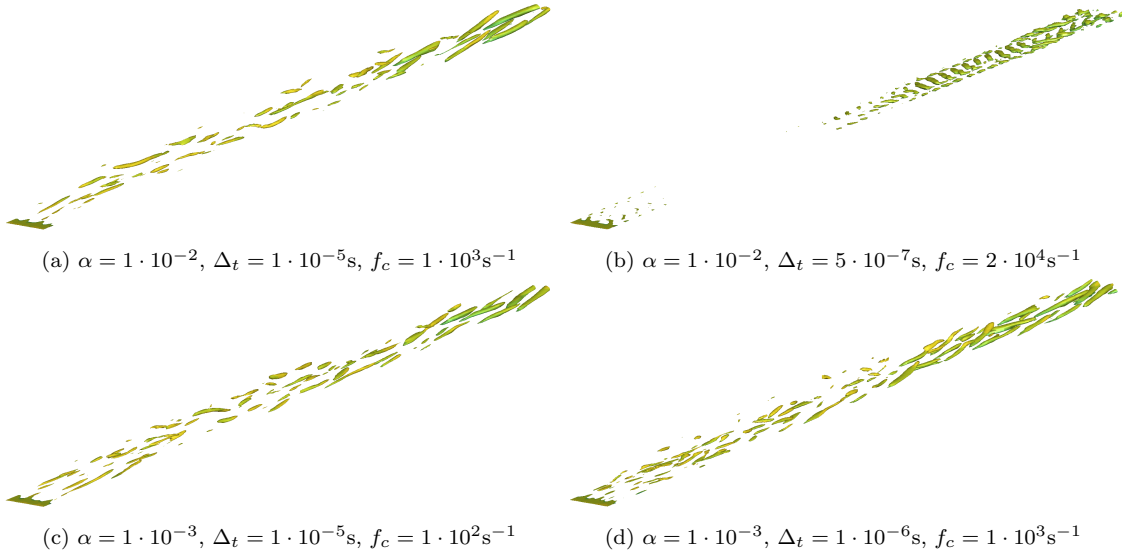

(a) $\alpha = 1 \cdot 10^{-2}$, $\Delta_t = 1 \cdot 10^{-5}$s, $f_c = 1 \cdot 10^{3}$s^{-1}

(b) $\alpha = 1 \cdot 10^{-2}$, $\Delta_t = 5 \cdot 10^{-7}$s, $f_c = 2 \cdot 10^{4}$s^{-1}

(c) $\alpha = 1 \cdot 10^{-3}$, $\Delta_t = 1 \cdot 10^{-5}$s, $f_c = 1 \cdot 10^{2}$s^{-1}

(d) $\alpha = 1 \cdot 10^{-3}$, $\Delta_t = 1 \cdot 10^{-6}$s, $f_c = 1 \cdot 10^{3}$s^{-1}

Figure 10: Time discretization: $Q = 1 \cdot 10^{6}$s^{-2} isosurface on mesh `x210` (see table 1) for cases `x210` / `ts1e-5`, `ts5e-7`, `a1e-3`, and `a1e-3_ts1e-6` (see table 2)

that the scales targeted by the injection should be correlated with the mesh size to get the right amount and type of resolved turbulence. However, independent of the injection, the temporal resolution has to be sufficient to capture the resolved turbulence that the mesh requires (F_{DES} depends on the mesh size but not on Δt), otherwise the distribution of turbulence will be incorrect.

6.4 Limiting the injection of turbulence

Figure 11 presents the results obtained when the limiter in equation (10) is applied to the forcing method.

The results presented show that the limiter is successful in significantly reducing the overestimation of TKE on the finer meshes, compared with figure 5. This validates the principle of the limiter, since on finer meshes there is a large region where LES is supposed to be established and the injection should be reduced.

However, overestimation of the total energy still occurs on the `x420` mesh. The near-wall layer turbulence is underestimated, so it is likely that the time step is too large to resolve all the turbulence required on this fine mesh, like in figure 9e. But the limiter (10) is also too simplistic: in spatially developing boundary layers, like in most realistic flows, there is no equilibrium between subgrid-scale production and dissipation. A more accurate estimation of the subgrid viscous dissipation could improve the limiter.

7 Conclusion

A volume forcing method to stimulate the creation of resolved turbulence in the grey zone has been presented, which is intended to reduce the modeled stress

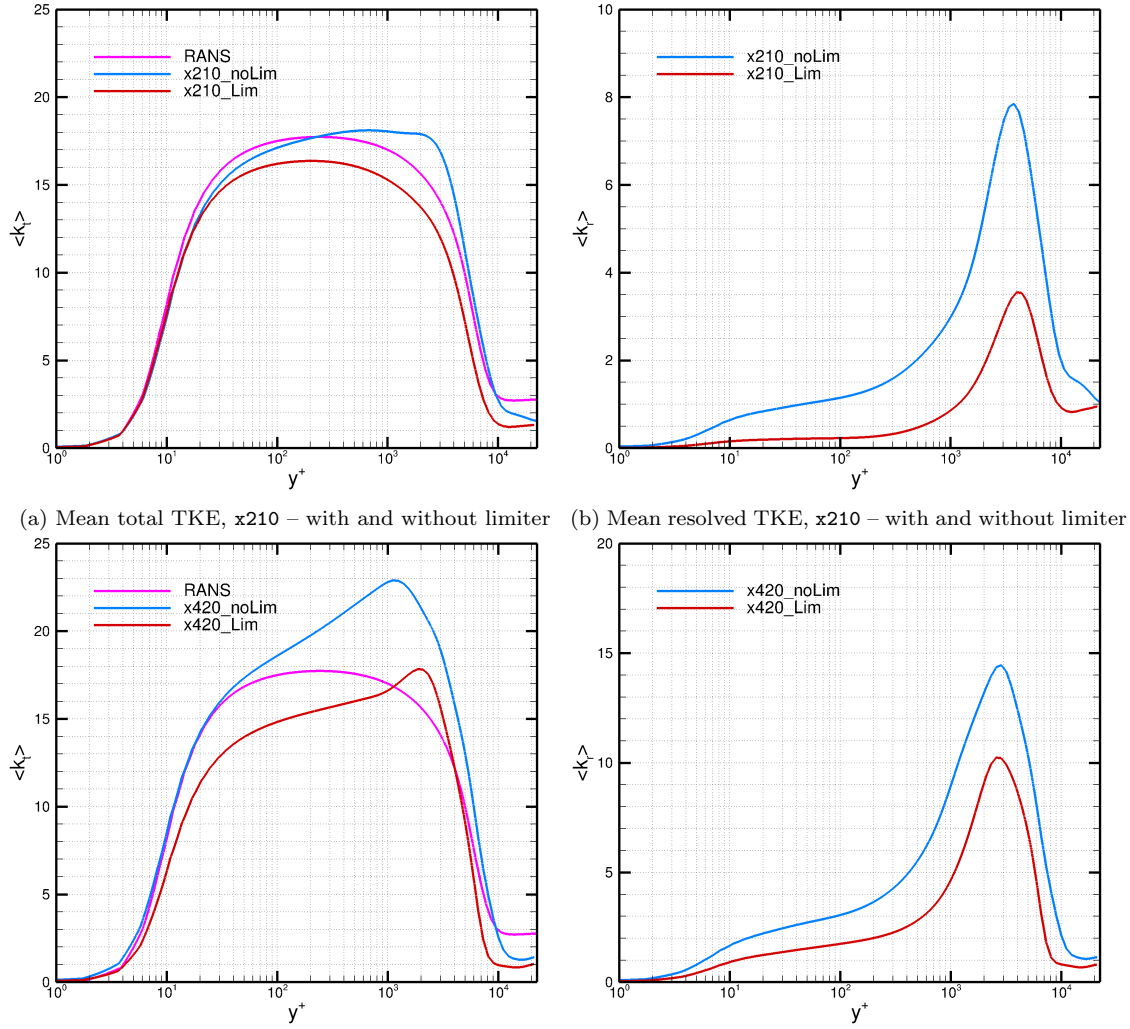

(a) Mean total TKE, `x210` – with and without limiter (b) Mean resolved TKE, `x210` – with and without limiter

(c) Mean total TKE, `x420` – with and without limiter (d) Mean resolved TKE, `x420` – with and without limiter

Figure 11: Impact of the limiting by the production term on the forcing method with meshes `x210` and `x420`

depletion issues of the DES-SST hybrid RANS/LES turbulence model. The forcing attempts to compensate for the artificial destruction of modeled TKE and is therefore based on the dissipation term of the k transport equation. The spectrum for the forcing is created by amplifying existing turbulence, following Lundgren's method. It was found that the forcing enhances the accuracy of the TKE and velocity profiles and allows for a much faster development of the boundary layer.

The forcing method proves to be sensitive to mesh variations, as finer meshes overestimate the amount of resolved turbulence in the flow. An attempt at limiting the injection of energy in the flow to remove the forcing once LES is established, significantly reduces the amount of resolved TKE for finer meshes but this limiter, based on the equilibrium of subgrid turbulence production and dissipation, is too approximate. A better alternative to estimate the subgrid viscous dissipation, based on an 'equilibrium' F_{DES} value for well-developed LES flow, is currently being worked on.

The injection also depends on variations of the filter size used to define the turbulent scales amplified by the forcing method. If these scales are too small, the

injected turbulence cannot be represented on the mesh and quickly disappears. Too large scales perturb the spectrum and may lead to overestimations. For optimal injection, a local correlation between the exponential smoothing coefficient α and the mesh size must be implemented. Such a correlation also allows to reduce the required user input.

However, apart from the forcing, the resolved TKE depends on the capacity of the mesh and time integration to sustain resolved eddies. Large time steps and stretched cells can perturb the distribution of TKE in boundary layers. Since RANS is far less sensitive to these issues than LES, it is always wise (if possible) to resolve attached boundary layers with RANS. The forcing must therefore be seen as a complement to shielding functions, rather than an alternative, and it would be interesting to combine the approach with for example DDES or IDDES.

A main advantage of the forcing approach is its simplicity, generality and relatively low computational costs, which mean that the method can be used to simulate more complex flows. Furthermore, it is not limited to boundary layers, but can also accompany changes in the turbulence distribution due to local spatial or temporal variations in the mesh size, which occur on unstructured and adaptively refined grids. Therefore, it could become an important component of an adaptive HRL simulation approach.

Acknowledgement

The computations were performed using HPC resources from GENCI (Grand Equipement National de Calcul Intensif) (Grant-A0082A00129, Grant-A0102A00129) which is gratefully acknowledged.

References

Arvidson, S., L. Davidson, and S.-H. Peng (2018). "Interface methods for grey-area mitigation in turbulence-resolving hybrid RANS-LES". In: *International Journal of Heat and Fluid Flow* 73, pp. 236–257.

Cahuzac, A., J. Boudet, P. Borgnat, and E. Lévêque (2010). "Smoothing algorithms for mean-flow extraction in large-eddy simulation of complex turbulent flows". In: *Physics of Fluids* 22(12), p. 125104.

Chaouat, B. and R. Schiestel (2005). "A new partially integrated transport model for subgrid-scale stresses and dissipation rate for turbulent developing flows". In: *Physics of Fluids* 17(6), p. 065106.

Girimaji, S. S. and K. Abdol-Hamid (2005). "Partially-Averaged Navier Stokes Model for Turbulence: Implementation and Validation". In: 43rd AIAA Aerospace Sciences Meeting and Exhibit. American Institute of Aeronautics and Astronautics: Reno, Nevada.

Girimaji, S. S. and S. Wallin (2013). "Closure modeling in bridging regions of variable-resolution (VR) turbulence computations". In: *Journal of Turbulence* 14(1), p. 72–98.

Kok, J. C. (2017). "A Stochastic Backscatter Model for Grey-Area Mitigation in Detached Eddy Simulations". In: *Flow, Turbulence and Combustion* 99(1), pp. 119–150.

Kraichnan, R. H. (1970). "Diffusion by a Random Velocity Field". In: *Physics of Fluids* 13(1), p. 22.

Lund, T. S., X. Wu, and K. D. Squires (1998). "Generation of Turbulent Inflow Data for Spatially-Developing Boundary Layer Simulations". In: *Journal of Computational Physics* 140(2), p. 233–258.

Lundgren, T. S. (2003). "Linearly forced isotropic turbulence". In: *Annual Research Briefs of Center for Turbulence Research*, p. 461–473.

Mehta, M., R. Manceau, V. Duffal, and B. de Laage de Meux (2023). "An active hybrid Reynolds-Averaged Navier-Stokes/Large Eddy Simulation approach for grey area mitigation". In: *Physics of Fluids*.

Menter, F. R. (1993). "Zonal Two Equation k-omega Turbulence Models for Aerodynamic Flows". In: 24th Fluid Dynamics Conference. Orlando, Florida, p. 22.

Mozaffari, S., E. Guilmineau, M. Visonneau, and J. Wackers (2022). "Average-based mesh adaptation for hybrid RANS/LES simulation of complex flows". In: *Computers & Fluids* 232, p. 105202.

Pruett, C. D., T. B. Gatski, C. E. Grosch, and W. D. Thacker (2003). "The temporally filtered Navier–Stokes equations: properties of the residual stress". In: *Physics of Fluids* 15(8), pp. 2127–2140.

Queutey, P. and M. Visonneau (2007). "An Interface Capturing Method for Free-Surface Hydrodynamic Flows". In: *Computers & Fluids* 36(9), pp. 1481–1510.

Rajamani, B. and J. Kim (2010). "A Hybrid-Filter Approach to Turbulence Simulation". In: *Flow, Turbulence and Combustion* 85, p. 421–441.

Rosales, C. and C. Meneveau (2005). "Linear forcing in numerical simulations of isotropic turbulence: Physical space implementations and convergence properties". In: *Physics of Fluids* 17(9), p. 095106.

Shur, M. L., P. R. Spalart, M. K. Strelets, and A. K. Travin (2008). "A hybrid RANS-LES approach with delayed-DES and wall-modelled LES capabilities". In: *International Journal of Heat and Fluid Flow* 29(6), p. 1638–1649.

Spalart, P. R., S. Deck, M. L. Shur, K. D. Squires, M. K. Strelets, and A. Travin (2006). "A New Version of Detached-Eddy Simulation, Resistant to Ambiguous Grid Densities". In: *Theoretical and Computational Fluid Dynamics* 20(3), pp. 181–195.

Spalart, P. R., W.-H. Jou, M. Strelets, and S. R. Allmaras (1997). "Comments on the Feasibility of LES for Wings, and on a Hybrid RANS/LES Approach". In: *First AFOSR International Conference on DNS/LES*. Ruston, Louisiana, p. 11.

Strelets, M. (2001). "Detached eddy simulation of massively separated flows". In: *39th Aerospace Sciences Meeting and Exhibit*. American Institute of Aeronautics and Astronautics: Reno, Nevada, p. 18.

Visonneau, M., E. Guilmineau, and G. Rubino (2020). "Local Flow around a Surface Combatant at Various Static Drift Angles: The Role Played by Turbulence Closures". In: *33rd Symposium on Naval Hydrodynamics*. online.